Volume 1 | Number 1 | Jan 2013 | Pages 1–100

PCCP

Physical Chemistry Chemical Physics
www.rsc.org/pccp

ROYAL SOCIETY OF CHEMISTRY

ROYAL SOCIETY OF CHEMISTRY

www.rsc.org/pccp

Fuel mediated solution combustion synthesis of ZnO supported gold clusters and nanoparticles and their application to catalytic activity and *in-vitro* cytotoxicity

T. Inakhunbi Chanu, Thangavelu Muthukumar and Periakaruppan T. Manoharan*

Department of Chemistry, Indian Institute of Technology/Madras, Chennai 600036 India

*Corresponding Author

Email: ptm@iitm.ac.in

Phone: +91 44 2257 4931

Fax: +91 44 2257 0509/0545

Abstract

Nanocomposites of gold nanoparticles and semiconductor ZnO with wurtzite structure, made by solution combustion synthesis (SCS), as a function of Zn/Fuel ratio with polyethylene glycol, PEG, as fuel exhibit the presence of both nanoparticles and clusters. Atomic gold clusters present on the surface of ZnO nanorods though can be identified by XPS and SEM are easily monitored and characterized by positive ion MALDI experiments as mostly odd numbered clusters, Au_3 to Au_{11} in decreasing amounts. Lowest fuel produces AuClO and nanoparticles, NP's, with no clusters. Au/ZnO at all [Au] exhibit single blue shifted plasmon absorption and corresponding photoluminescence (PL). Increasing particle size prefers surface plasmon resonance (SPR) scattering of metal that could lead to PL enhancement; however, available ZnO surface in the Au/ZnO composite becomes more important than the particle size of the composite with higher [Au]. The catalytic activity of this nanocomposite Au/ZnO tested on 4-nitophenol clearly revealed the presence of an intermediate with both NP's and clusters playing different roles. An *in vitro* study of cytotoxicity on MCF-7 cell lines reveals that these gold nanostructures have turned out to be powerful nanoagents for destruction of cancer cells even with small amounts of gold particles/clusters. The nanorods of ZnO, known to be nontoxic to normal cells, play a lesser part in anticancer activity of these Au/ZnO nanocomposites.

Key words: Au/ZnO Nanocomposites, gold nanoparticles, gold clusters, surface plasmon resonance, photoluminescence, MALDI, catalytic activity, cytotoxicity, MCF-7 Cell lines

1. Introduction

Nanomaterials smaller than 2 nm have received a considerable interest in recent years due to their size and shape dependent catalytic, optical and electronic properties which are quite different from their bulk materials.[1-3] Such smaller nanoparticles which are made up of few to hundred atoms per particle are termed as atomic clusters. Compared to bulk nanomaterials, clusters have a larger number of atoms on the surface of the composites. Also, the continuum bands observed in bulk nanomaterials get modified into discrete energy levels due to the quantum confinement of electron and hole.[4] Among the metal clusters, Au clusters show potential applications in various fields such as catalysis, sensor and biological labeling,[5-7] and on the basis of number of atoms present in cluster, they show unique optical and physical properties.[8-10] The advantage of Au cluster over other metal clusters is their low toxicity that has made them suitable candidates for biomedical application.[11] Therefore, development of methods for the synthesis of Au cluster is important. Brust *et al*.[12] introduced the preparation of thiol protected Au cluster by two phase method. Subsequently several Au clusters have been synthesized by various methods.[13-16] Rath *et al*.[13] reported Au_8 cluster with a planar hexagonal shaped using surfactant mediated chemical technique. Shibu *et al*.[14]synthesized the NIR emitting glutathione protected Au_{22} clusters. A lysozyme stabilized fluorescent Au cluster was used as a sensor for selective detection of Hg^{2+}.[17] In this article, we report the formation of Au cluster deposited on the ZnO nanocomposites using solution combustion synthesis (SCS). SCS offers several advantages over other methods which include high energy and time-efficient process leading to a simple and cost effective method. For instance, the high reaction temperature generated during the combustion process results in the formation of finely dispersed and porous morphology of the products.[18] Another advantage of SCS lies in the ability to chemically modify the properties of products just by changing the ratio of metal ion and fuel precursor. In SCS,

metal nitrate serves as an oxidizer and the organic fuel as a reducing agent. Many organic compounds such as glycine, thiourea, urea, polyethylene glycol (PEG) etc. have been used as a reducing agent.[19-22] These compounds differ in the reducing power and the amount of gases they generate. The particle size, morphology and optical properties of the particles depend on type of fuel employed and also on the ratio of oxidizing and reducing agents used during the combustion synthesis. It has been reported that the optical properties of semiconductor materials improve significantly on coupling with the surface plasmon (SP) based noble metals. A 14 fold photoluminescence (PL) enhancement of InGaN/GaN quantum well was observed by capping with Ag due to SP mediated emission.[23] Many other semiconductor metal nanocomposites such as Ag-ZnO, Au-ZnO, Al-ZnO and Pt-ZnO were studied to investigate the energy transfer between semiconductor and SP energy of metal.[24-27] Herein, the roles of fuel on the cluster formation and optical properties of Au-ZnO have been investigated. PEG was used as fuel on the synthesis of pure ZnO and Au-ZnO nanocomposites. To examine the catalytic activity of metal nanoparticles, many works have been reported on the reduction of nitro compound into amino derivatives using metal nanoparticles as a catalyst.[28-31] In this article, we analyzed the catalytic activity of Au-ZnO nanocomposites by studying the reduction of 4-Nitrophenol (4-NP) with $NaBH_4$ in the absence and presence of Au-ZnO nanocomposites. The current findings will show the importance of fuel and percentage of doping to get desired Au-ZnO nanocomposites. In addition our work is able to predict the course of the reduction process with differential roles of both nanoparticles and clusters. In addition the gold clusters and nanoparticles on the surface of ZnO have anticancer characteristics.

2. Experimental Details

2.1. Chemicals

$Zn(NO_3)_2.6H_2O$ (Qualigens), $NaBH_4$, Polyethyleneglycol (Merck), $HAuCl_4.3H_2O$, 4-Nitrophenol (laboratory reagent), Methanol (SRL) and Dithranol, Dihydroxybenzoic acid, Sinnapinic acid were procured from Aldrich. All other reagents were of analytical grade. Millipore water was used for all analysis.

2.2. Instrumentations

Samples were characterized by different techniques. X-ray powder diffraction measurements were recorded using X-ray diffractometer (Bruker D8 ADVANCE) using $CuK\alpha$ (λ= 0.1548 nm) radiation. DRS UV-visible spectra for all the samples were measured in evolution 600 UV-Vis Spectrophotometer using $BaSO_4$ as a reference. X-ray Photoelectron spectra (XPS) were measured using Omicrometer Nanotechnology instrument. UV-visible absorption spectra were recorded using a Perkin-Elmer Lambda 25 instrument. PL measurements were acquired using Jobin Yvon Flurolog-3-11 Spectroflurometer. The morphology and composition of samples were recorded by Field Emission Scanning Electron Microscopy (FE-SEM, F E I Quanta FEG 200 - High Resolution Scanning Electron Microscope) equipped with energy dispersive X-ray analysis (EDX). High Resolution Transmission Electron Microscopy (HRTEM) JEOL 3010 operated at 300 kV was used for the identification of size and lattice fringes of the samples. Matrix assisted laser desorption time of flight (MALDI-TOF) mass spectra were acquired on a Bruker Ultraflextreme equipped with a pulsed IR laser with 337 nm. All mass spectra were acquired in the positive reflection mode. EPR spectra both at room temperature (300 K) and liquid nitrogen temperature (77 K) were recorded on BRUKER N500 EPR spectrometer.

2.3. Methodology

2.3.1. Synthesis and Characterization

Nanocrystalline ZnO was prepared by SCS method reported earlier by our group.[32] In brief, Zn $(NO_3)_2$ was used as the Zn source and PEG as the fuel. It involves direct mixing of a desired molar ratio of $Zn(NO_3)_2$ and PEG. The ratio of $Zn(NO_3)_2$ to PEG was varied from 3 to 30 depending on the desired products, varying the molar ratio. After mixing $Zn(NO_3)_2$ and PEG uniformly, the mixture was transferred to a muffle furnace preheated to 450°C for ignition. The reaction lasted for less than ten minutes produced dry ZnO nanocrystals. The synthesized material was further kept at the same temperature for another 20 min. Different concentration of Au-ZnO nanocomposites were also synthesized by the same procedure with $HAuCl_4$ as Au source. After completion of the reaction, the samples were washed with millipore water for several times and then with methanol in order to remove the impurities. The synthesized materials were finally calcined at 500°C for 30 min. The prepared samples have been designated as 0.2% Au-ZnO, 0.5% Au-ZnO, 1% Au-ZnO and 5%Au-ZnO respectively for the compositions, $Au_{0.002}Zn_{0.998}O$, $Au_{0.005}Zn_{0.995}O$, $Au_{0.010}Zn_{0.99}O$ and $Au_{0.050}Zn_{0.95}O$.

For MALDI-TOF measurements, 2 μL of the nanoparticle suspension prepared in 10 μL of 0.1% TFA was mixed with 2 μL of dithranol matrix, and then the 0.2 μL of the mixture was deposited on the MALDI plate and allowed to air dry before the MALDI-TOF MS measurements.

2.3.2. Catalytic Reduction

The catalytic reduction reaction was carried out in10 ml volumetric flask. In a typical reaction 8 ml of 0.1mM solution of 4-NP was mixed with 2 ml of 15 mM ice cold $NaBH_4$ solution. This was followed by the addition of 50 mg of Au-ZnO NPs and was stirred for a regular interval of time. Then the solution was centrifuged and supernatant solution was recorded for UV-Visible absorption measurements in a scanning range of 200 - 600 nm at room temperature and 50°C.

2.3.3. *In vitro* assay for cytotoxic behaviour (MTT assay)

The 3-(4,5-dimethylthiazol-2-yl)-2,5-diphenyltetrazolium bromide (MTT) assay was carried out to determine the viability of cells based on the reductive cleavage of MTT (a yellow salt) to formazan (a purple compound) by mitochondrial dehydrogenase of living cells. Cytotoxicity of samples on MCF-7 (cancer cell line was obtained from National Centre for Cell Sciences (NCCS), Pune) was determined by the MTT assay.[33] Cells (1×10^5/well) were plated in 1 ml of RPMI medium/well in 24-well plates. After 48 h of incubation, the cell reaches the confluence. Cells were then incubated in the presence of various concentrations of the samples of nanoparticles/clusters (6, 12, 25, 50, 100 and 200 µg per well) which were prepared under different ZnO/PEG fuel ratios for 48 h at 37°C in CO_2 incubator. After the removal of sample solution the wells containing left-over live cells were carefully washed with PBS (pH 7.4). To this was added 200 µl/well (5 mg/ml) of 0.5% MTT /PBS solution and incubated for 4 h which was followed by the addition of 0.04 M HCl/isopropanol. Spectrophotometric absorbance of the purple blue formazan dye was measured in a microplate reader at 570 nm (Biorad 680). Measurements were performed and the concentration required for a 50% inhibition of viability (IC50) was determined graphically. The sample without any cells served as a blank. The effect of the samples on the proliferation of MCF-7 was expressed as the % cell viability. A control was performed with 3T3 fibroblast cells.

3. Results and discussion

3.1. XRD studies reveal the importance of fuel concentration on the formation of Au clusters

Figure 1a shows the XRD patterns of the pure ZnO and Au-ZnO nanocomposites where the Zn/PEG ratio was kept at 30 but varying the Au concentration from 0 to 5%. The entire

diffraction pattern is well assigned to ZnO and Au according to JCPDS Card No. 36-1451   and

65-2870 respectively. ZnO exhibit wurtzite and Au in face centre cubic (fcc) structures

respectively. The average crystallite sizes in the ZnO and Au-ZnO samples were estimated using

the Debye Scherrer equation. The particle size of the pure ZnO and 5% Au-ZnO was calculated

to be 28 nm and 18 nm according to (100) plane of ZnO. Based on the relative intensities of the

two large peaks due to Au(111) and ZnO(101) at $2\theta=38.2$ and 36.2 respectively, the ratio of Au

to ZnO peak was calculated to be 0.09, 0.14, 0.25 and 1.11 for 0.2%, 0.5%, 1% and 5% Au-ZnO

nanocomposites. This observation of continuous increment in the value for Au in relation to ZnO

indicates that at high concentration of Au, most of the Au particles are deposited on the surface

of ZnO. We have also carried out experiments to see the effect of calcination. Figure 1b shows

the XRD pattern of pre-calcined 5% Au-ZnO nanocomposite prepared at Zn/PEG ratio of 30. It

can be seen that the intensity of ZnO peak was drastically reduced and Au peak appeared

maximum and the ratio of Au to ZnO peak was calculated to be 2.40, which is much higher for

the corresponding calcined sample. In addition, there is an emergence of new peak at $2\theta =12$ and

a 'doublet' looking smaller peaks at $2\theta = 33$ and 34. An enlarged version of the $2\theta \sim 28$-37

region as shown in the insert of Figure 1b clearly pictures these two new peaks. These peaks at

$2\theta = 12$, 33, 34 were also observed in the calcined 5% Au-ZnO, however with drastically

reduced intensities in the latter case. These peaks match with the JCPDS No 850377, which

correspond to AuClO, the presence of which was also seen by MALDI experiment (vide infra).

In the case of pre-calcined sample, it was possibly difficult to remove the Cl trapped inside the

particle and hence the formation of AuClO is most possibly an indication of the initial reaction of

$AuCl_4^{-1}$ with water prior to the formation of Au clusters through oxidation by $Zn(NO_3)_2$.

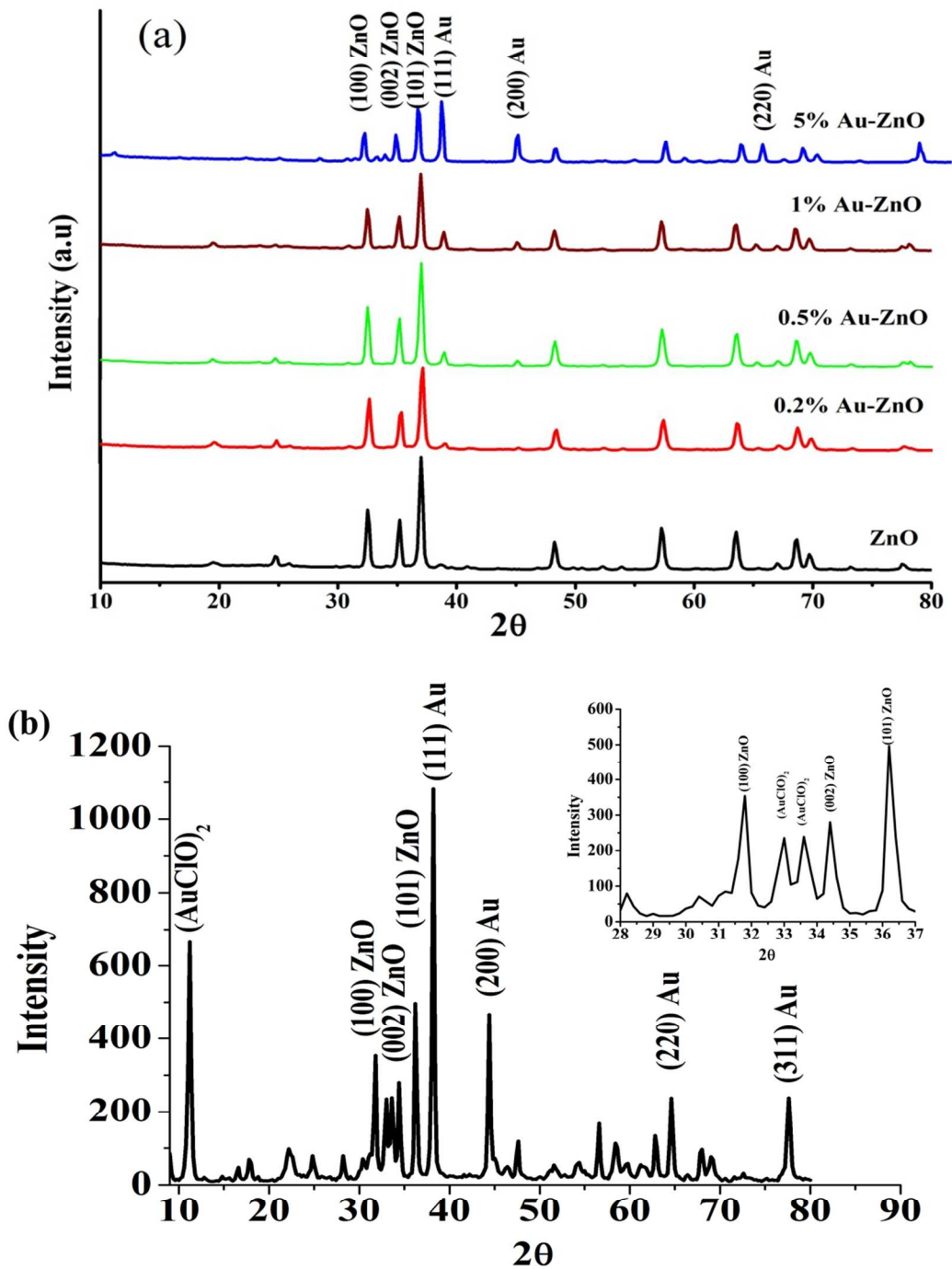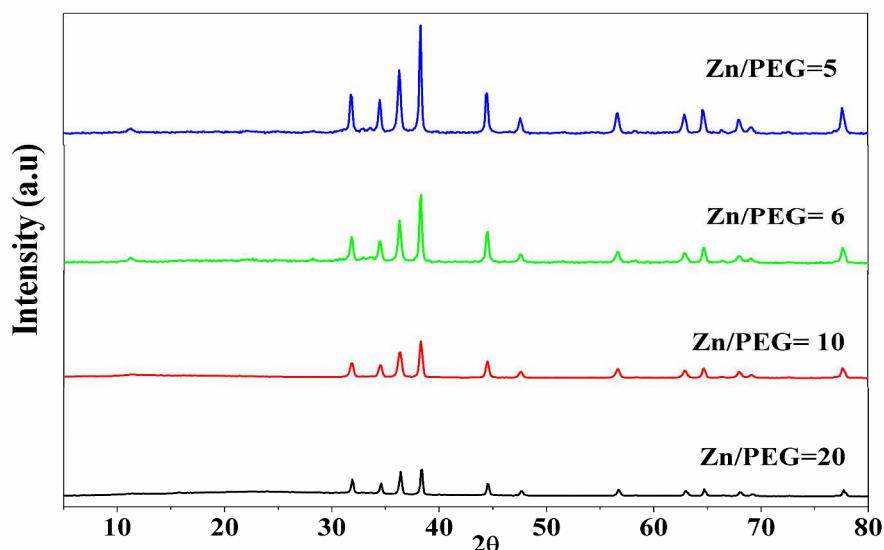Therefore, we carried out all the measurements with the calcined samples.

Figure 1. **(a)** **X-Ray diffraction patterns of pure ZnO and Au-ZnO nanocomposites prepared at Zn/PEG ratio of 30, (b) X-Ray diffraction pattern of pre calcined 5% Au-ZnO. Inset picture show the enlarged XRD peaks between 2θ = 30 and 36.**

Figure 2. X-Ray diffraction patterns of calcined 5% Au-ZnO nanocomposites prepared at different Zn/PEG ratio.

To determine the effect of fuel concentration, 5% Au-ZnO nanocomposite was prepared at different Zn precursor to PEG ratio. Figure 2 shows the XRD pattern of calcined 5% Au-ZnO at different Zn/PEG ratio. In this case also, peak at $2\theta = 12$ was observed but its intensity was considerably reduced on increasing PEG concentration (supporting info T1). This suggests that the formation of Cl containing Au nanoparticles was reduced on increasing PEG concentration i.e., lower Zn/PEG ratio and the intensity ratio of Au to ZnO peak was increased. The ratio of Au to ZnO peak was calculated to be 1.14, 1.41, 1.62 and 1.67 for Zn/PEG ratio of 20, 10, 6 and 5. At Zn/PEG ratio of 3, the intensity ratio of Au to ZnO was found to be 1.22 which is lower than the Zn/PEG ratio of 5 (supporting info S1).This shows that the formation of Au nanoparticles depend on the amount of PEG concentration. At high PEG, the presence of unburnt carbon may hinder the formation Au-ZnO nanocomposites. Therefore, we kept the PEG concentration between Zn/PEG of 30 to 5 only. In addition to Au nanoparticles deposited on ZnO, the presence of Au clusters can also be identified from XRD data through the broadening of diffraction peaks. Wu and co-workers explained the broadening in the XRD peaks due to the presence of clusters.[34]

It can be seen in our present studies that the XRD of 5%Au-ZnO at $2\theta = 38.2$ which correspond to (111) plane of Au was broadened on decreasing the Zn/PEG ratio (Supporting info S2). This indicates the formation of Au clusters in addition to Au nanoparticles deposited on ZnO.

3.2. Presence of atomic Au clusters on the surface of ZnO as revealed by XPS and EPR

XPS technique was used to further characterize the pure ZnO and Au-ZnO nanocomposite. Binding energy was calibrated by taking C 1s peak (284.9 eV) as a reference. Deconvolution of XPS spectra of Au 4f- Zn 3P are shown in Figure 3. It was resolved into four peaks at 83.4, 87.3, 88.7 and 91.6 eV respectively, which correspond to Au $4f_{7/2}$, Au $4f_{5/2}$, Zn $3p_{3/2}$ and Zn $p_{1/2}$.[35] For the samples prepared at Zn/PEG ratio of 30, a small amount of Au peak was observed at 0.5% Au-ZnO (Figure 3a) and, however, Au peaks were prominently observed at 5% Au-ZnO (Figure 3b). Peaks at 85.9 and 89.6 can also be seen in addition to Au 4f and Zn 3p peaks in the case of 5% Au-ZnO. These peaks match with $4f_{7/2}$ and $4f_{5/2}$ of Au^{3+}.[36] Also a peak at 200 eV due to Cl $2p_{3/2}$ was observed (supporting info S3).Therefore, the formation of AuClO is again supported from XPS spectra of 5% Au-ZnO. For same composition prepared at lower Zn/PEG ratio, i.e., 5% Au-ZnO at Zn/PEG ratio of 5 (Figure 3c), the intensity of Au peak was found to be more than that for Zn/PEG ratio of 30 whereas the peaks for Au^{3+} could not be resolved due to low amount of AuClO present in the sample. This again supports the XRD result of the formation of larger amount of Au nanoparticles with decreasing Zn/PEG ratio, suggesting the need for adequate supply of energy for the formation of Au nanoparticles.
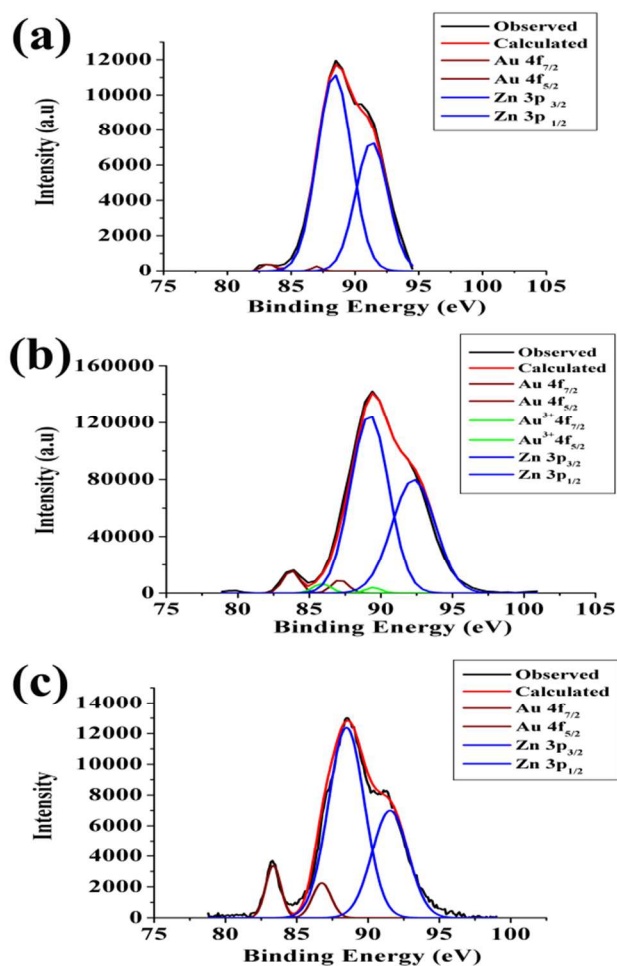
Figure 3. Photoelectron spectra of Au-ZnO (a) 0.5% Au-ZnO prepared at Zn/PEG ratio of 30 (b) 5% Au-ZnO prepared at Zn/PEG ratio of 30 (c) 5% Au-ZnO prepared at Zn/PEG ratio of 5.
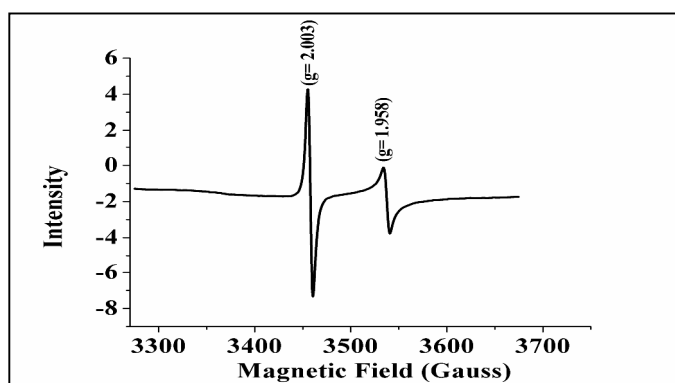

Figure 4. Room Temperature Electron Paramagnetic Resonance of 5% Au-ZnO nanocomposites prepared at Zn/PEG ratio of 6.

The room temperature electron paramagnetic resonance (EPR) of 5% Au-ZnO nanocomposites prepared at Zn/PEG ratio of 6 is shown in Figure 4. It can be seen that there was a presence of two isotropic peaks at g-values of 2.003 and 1.958 with no hyperfine lines. The g value at 1.958 is attributed to electrons in conduction band of ZnO and not from the O vacancies.[32] The atomic Au with an unpaired electron in 5s orbital shows EPR signal at g = 2.004.[37] Therefore the g value at 2.003 observed in our present studies must be from Au nanoparticles and/or clusters present on the surface. The 5s orbital must be present as a 5s band since there is proof for the formation of nanocrystals and nanoclusters (vide infra).

3.3. Rod like Morphology of pure ZnO changes to disc shape during Au deposition

Figure 5 shows the scanning electron microscopic (SEM) images and energy dispersive X-ray analysis (EDX) of pure ZnO and Au-ZnO nanocomposites. Pure ZnO shows rod like nanostructure (Figure 5a) with a diameter of 80 nm, the EDX showing the presence of only Zn and O. It can be seen from the SEM images of 5% Au-ZnO (Figure 5b and c) that there is a deposition of Au on the surface of ZnO with a disc shaped nanostructures. The EDX (Figure 5e) of pre-calcined 5% Au-ZnO prepared at Zn/PEG ratio of 30 shows a substantial presence of Cl in addition to Au, Zn and O peaks, the Cl being only from AuClO (Figure 5e). This is in agreement with XRD (Figure 1b) and also XPS. However, Cl peak was substantially absent in all cases of calcined samples inclusive of 5% Au-ZnO prepared at Zn/PEG ratio of 5 shown in Figure 5f again in accord with the XRD results. It can also be seen from EDX spectra that the amount of Au at Zn/PEG of 30 was more in the pre-calcined samples than not only the calcined samples prepared with Zn/PEG ratio of 30 but also those prepared at Zn/PEG of 5.
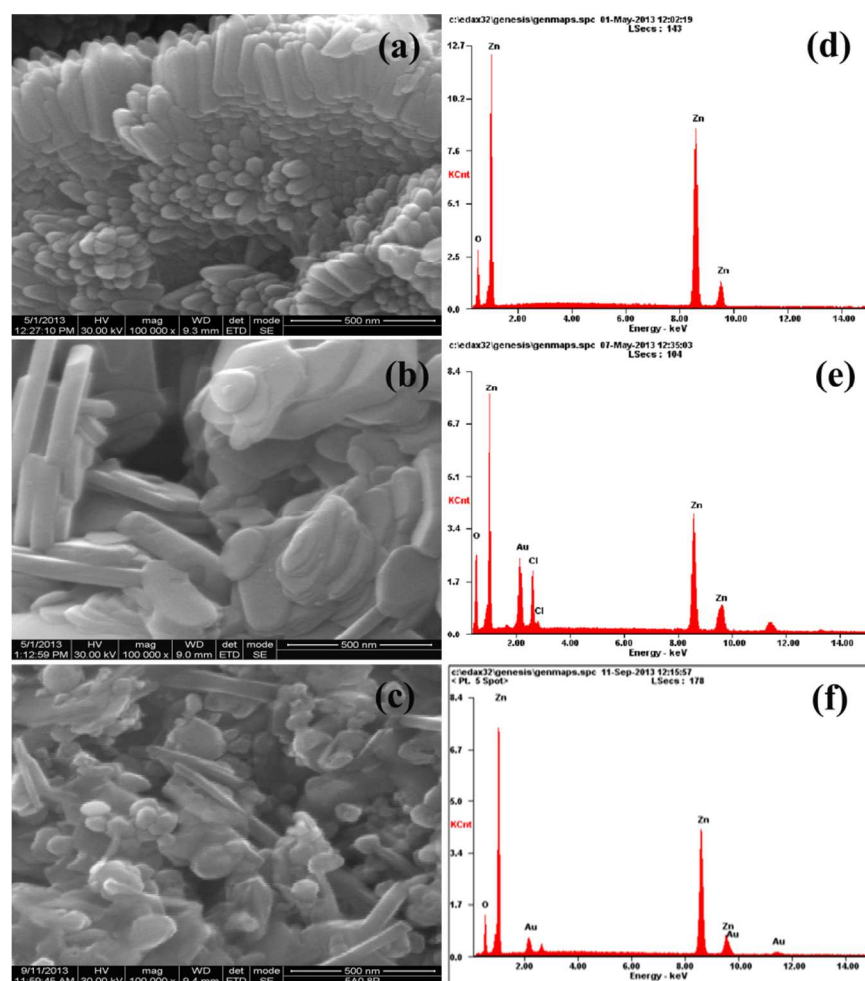
Figure 5. SEM images of (a) ZnO (calcined) (b) 5% Au-ZnO both with Zn/PEG ratio of 30 (precalcined) and (c) calcined 5% Au-ZnO of Zn/PEG ratio of 5, and their corresponding EDX (d), (e) and (f).

High resolution transmission electrons microscopic (HRTEM) images of pure ZnO and Au-ZnO nanocomposites are shown in Figure 6. The presence of lattice fringes clearly proves the material to be crystalline. The high resolution image of pure ZnO (Figure 6a) with d spacing of 2.75Å corresponds to (100) plane as found in XRD. The HRTEM of Au-ZnO nanocomposite (Figure 6 b) shows the d spacing of 2.75Å and 2.3Å, the former corresponding to the ZnO (100) plane and the latter to Au (111) plane. From the TEM image of the 5% Au-ZnO prepared at Zn/PEG ratio of 5 (Figure 7), the average particle size was calculated to be 25 nm which is larger than the one

calculated from the XRD. This may be due to the agglomeration during drying process. The presence of Au clusters can also be seen from the enlarged TEM image (Figure 7) in addition to the larger Au nanoparticles, as supported by the results of XRD and MALDI (vide infra) the latter clearly revealing the formation of Au clusters.
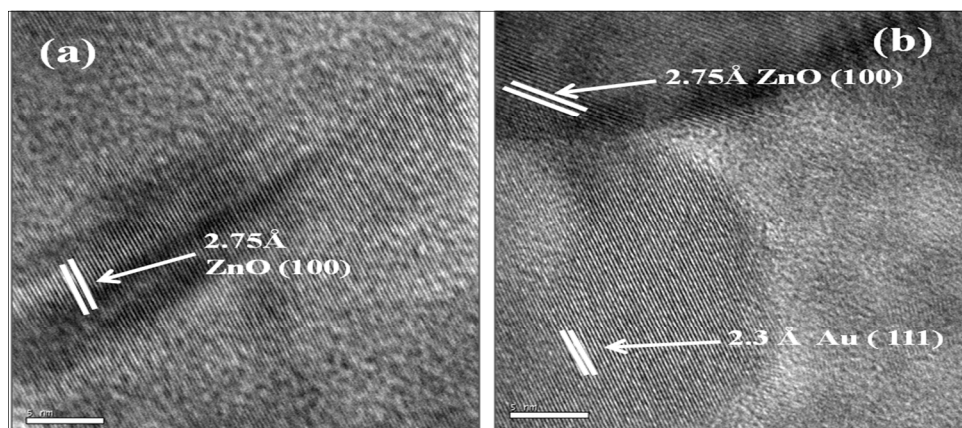
Figure 6. HRTEM image of (a) pure ZnO with Zn/PEG of 30 and (b) 5% Au-ZnO of Zn/PEG 5.
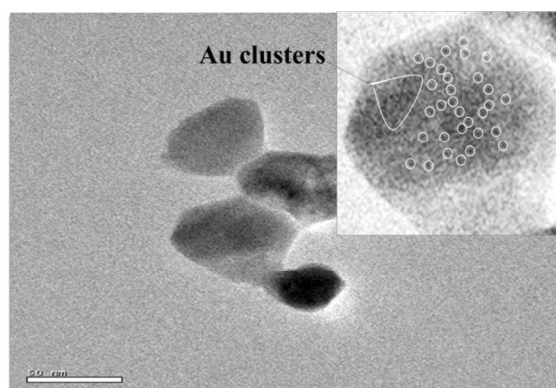
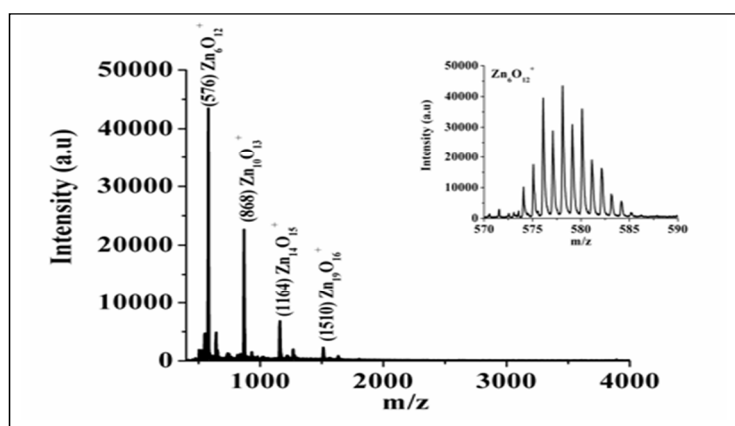**Figure 7. TEM image of 5% Au-ZnO prepared at Zn/PEG ratio of 5. Inset picture with rounded dark spots give the enlarged image showing the presence of Au clusters.**

3.4 MALDI-TOF monitors and characterizes the Au atomic clusters

A study of matrix assisted laser desorption time of flight (MALDI TOF) mass spectra was carried out on pure ZnO and Au-ZnO nanocomposites in order to identify the formation of

Au clusters on ZnO surface. Dithranol was used as a matrix. We also tried sinnapinic acid and dihdroxybenzoic acid as a matrix, however we couldn't observe ion peaks in these latter matrices. When dithranol was used as matrix, very fine ion peaks were observed. Similar observation was reported where the use of dithranol as a matrix yielded TiO_2 ion peaks and none of other organic matrices gave TiO_2 ion peaks.[38] This was explained due to the absence of strong acidic group in dithranol. Figure 8 shows the MALDI TOF mass spectra of pure ZnO. There was a series of peaks observed in the range of m/z 500 to 2000. Major peak was observed at m/z 576 corresponding to $Zn_6O_{12}^+$ and m/z 868 to $Zn_{10}O_{13}^+$. A cluster of $Zn_{14}O_{15}^+$ and $Zn_{19}O_{17}^+$ were also observed as minor peaks. Inset shows enlarged mass spectra at m/z 576. It can be seen that the peak consists of small peaks separated by one unit. This is attributed to the isotropic distribution in $Zn_6O_{12}^+$ cluster since atomic Zn exists in five different stable isotopes as ^{64}Zn, ^{66}Zn, ^{67}Zn, ^{68}Zn, and ^{70}Zn. Similar observation has been reported on MALDI-TOF of isotropic distribution of TiO_2 cluster.[39] Isotopic distributions are also noted in the other $Zn_xO_y^+$ clusters mentioned above.

Figure 8. MALDI-TOF Mass Spectra (positive ions) of Pure ZnO. Inset: Isotopic distribution of $Zn_6O_{12}^+$.

Figure 9 shows the MALDI-TOF mass spectra of the 1% and 5% Au-ZnO prepared at Zn/PEG ratio of 30. At 1% Au-ZnO (Figure 9a), in addition to ZnO cluster peaks, there is also formation

of $Au_{n,m}$ clusters with n, m representing odd and even numbers. Au_3 appeared maximum along with the minute amounts of other $Au_{n,m}$ clusters. However, at the same ratio of Zn/PEG i.e. 30, the mass spectra of 5% Au-ZnO did not show any peaks due to Au clusters. Only ZnO cluster peaks along with a new peak at m/z 515 can be seen in the spectra. The peak at m/z 515 correspond to $(AuClO)_2$ cluster and this peak is made up of small peaks separated by one unit. Since Cl exist in two stable isotopes, ^{35}Cl and ^{37}Cl, this indicates the isotropic distribution of AuClO which is shown in inset Figure 9b.To determine the effect of fuel on the formation of Au clusters, the MALDI-TOF mass spectra measurements were carried out at lower Zn/PEG ratio.
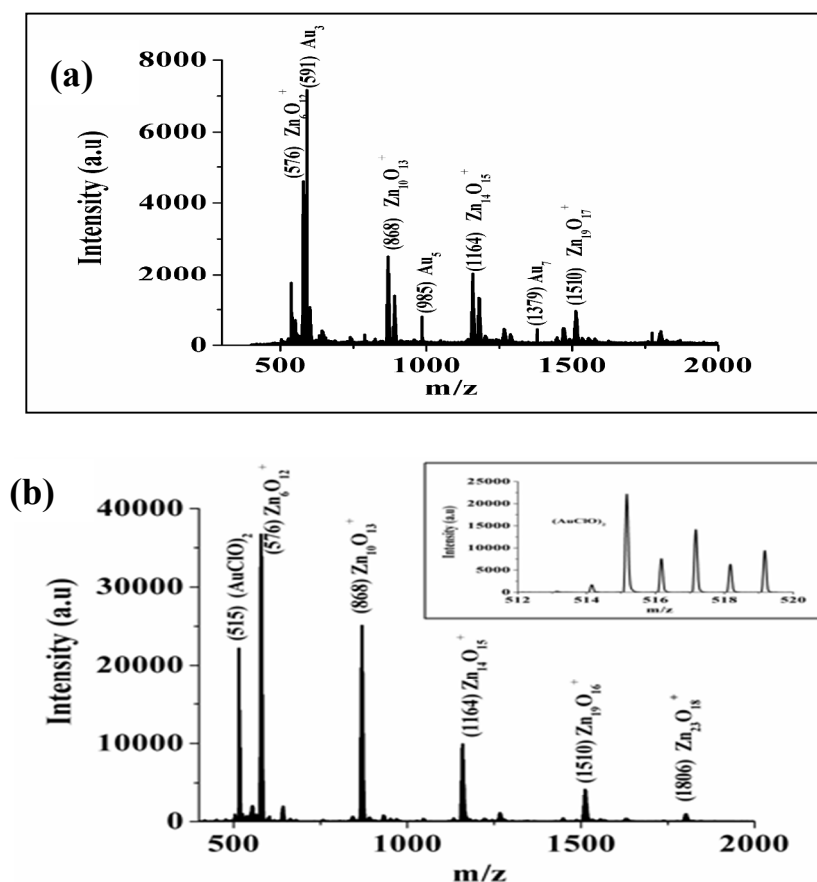
Figure 9. MALDI-TOF Mass Spectra (positive ions) of Au-ZnO prepared at Zn/PEG ratio of 30 at different Au concentration (a) 1% Au and (b) 5% Au. Inset in 9b: Isotopic distribution of $(AuClO)_2$ due to $^{35,37}Cl$.

Figure 10 shows the MALDI-TOF mass spectra of Au-ZnO prepared at different Zn/PEG ratio. It can be seen from the mass spectra of 5% Au-ZnO prepared at Zn/PEG ratio of 10 (Figure 10a) that there was a formation of series of Au_n clusters with odd number of gold atoms with n=3,5,7 and 9 with the maximum intensity for Au_3, along with some even number clusters Au_m with m = 4 and 6 with descending order of intensity. The total intensity of the even numbered clusters was much smaller than that of more abundant odd numbered ones, showing preference for the latter in this method of synthesis. There was no peak observed at m/z 515, which clearly indicates the absence of AuClO clusters. At Zn/PEG ratio of 6 and 5 also (Figure 10 b and c), the intensity of Au_3 cluster appeared maximum in addition to the presence of odd number larger Au cluster with n = 5,7,9,11,13 and even number larger Au cluster peaks with n= 4,6,8,10,12, with reduced in intensity as n and m increase. In this cases also, there was no peak observed at m/z 515 and ZnO peaks were drastically reduced. To see the effect of Au concentration, MALDI-TOF was recorded for 1% Au-ZnO prepared at Zn/PEG ratio of 5 (Figure 10d). It can be seen that similar numbers of Au clusters were being formed with maximum intensity at Au_3, however intensity of other peaks were drastically reduced. We have also recorded MALDI-TOF of 0.5% Au-ZnO and in this case, only ZnO clusters peak were predominant along with a very small amount of Au cluster peaks (supporting info S4). Therefore, the formations of Au clusters depend on the amount of PEG and percentage of Au used during preparation. The geometry of Au clusters have already been predicted by theoretical calculation.[39] They show that Au_3 cluster exists in triangular flat structure and Au_5 cluster have a preference to the isosceles trapeze structure. Similar structure might be occurring in our present studies where the Au_3 cluster exists in triangular flat structure.

Though it is true that the nature of Au clusters Au_n, Au_m, AuClO and Zn_xO_y clusters have been clearly identified, few interesting general observations have been made. Pure ZnO produces

only Zn_xO_y clusters with similar features in 1% and 5% Au-ZnO under Zn/Fuel ratio of 30 except for the formation of Au_3 with 1% Au-ZnO and $(AuClO)_2$ in 5% Au-ZnO. The latter probably indicates that most of Au is present as $(AuClO)_2$ with unobservable quantity of $Au_{n/m}$ clusters negating the XRD data, which is quite perplexing. The rest of the Au, hence, must have been present as Au crystalline nanoparticles. However, when the Zn/Fuel ratio is decreased to 10, 6 and 5, it is observed (i) clearly Au clusters only of the form Au_n and Au_m are formed where n and m are respectively even and odd; (ii) even numbered cluster formation is much less favored than the odd numbered ones; (iv) n and m taken together suggests all clusters are formed by the addition of one atom each, building up from Au_3 as the base which presents itself as the major species; (v) the preponderance of the odd numbered species can be explained according to work reported by Va´zquez group.[1] They also observed the formation of odd numbered Au clusters species with a maximum intensity at Au_3. This was explained due to the stable charged clusters with an even number of electron are more favored and so the majority of Au clusters are in the form of odd number of atoms per Au clusters; (vi) In all Au-ZnO nanocomposites, Au_3 remain the major cluster along with the presence of other larger number of Au clusters. The relative abundance of large Au clusters depends on the percentage of Au and Zn/PEG ratio used during preparation. The relative ratio of larger Au clusters with respect to Au_3 is shown in Supporting Information T2. It was observed that the relative abundance of Au_5, Au_7 and Au_9 was found to be minimum at 1% Au-ZnO prepared at Zn/PEG ratio of 30 and their relative abundance was found to be higher in 1% Au-ZnO prepared at Zn/PEG ratio of 5. The 5% Au-ZnO prepared at Zn/PEG ratio of 5, 6 and 10 also show the presence of Au_5, Au_7, Au_9 and Au_{11} with the lesser abundance than in 1% Au-ZnO of Zn/PEG 5. As we decrease the ZnO/PEG ratio with higher input of Au we observe substantially reduced amount of $Zn_nO_m^+$ ions revealing the deposition of gold on the

surface of ZnO which prevents the formation of the latter ions, in accordance with the results of XRD and XPS.

The above points suggest that there is a possibility to synthesize pure Au_n or one or two species with n being different, the latter of which could then be separated by some procedure by adjusting the fuel ratio and the concentration of $HAuCl_4^-$. This work is under progress.
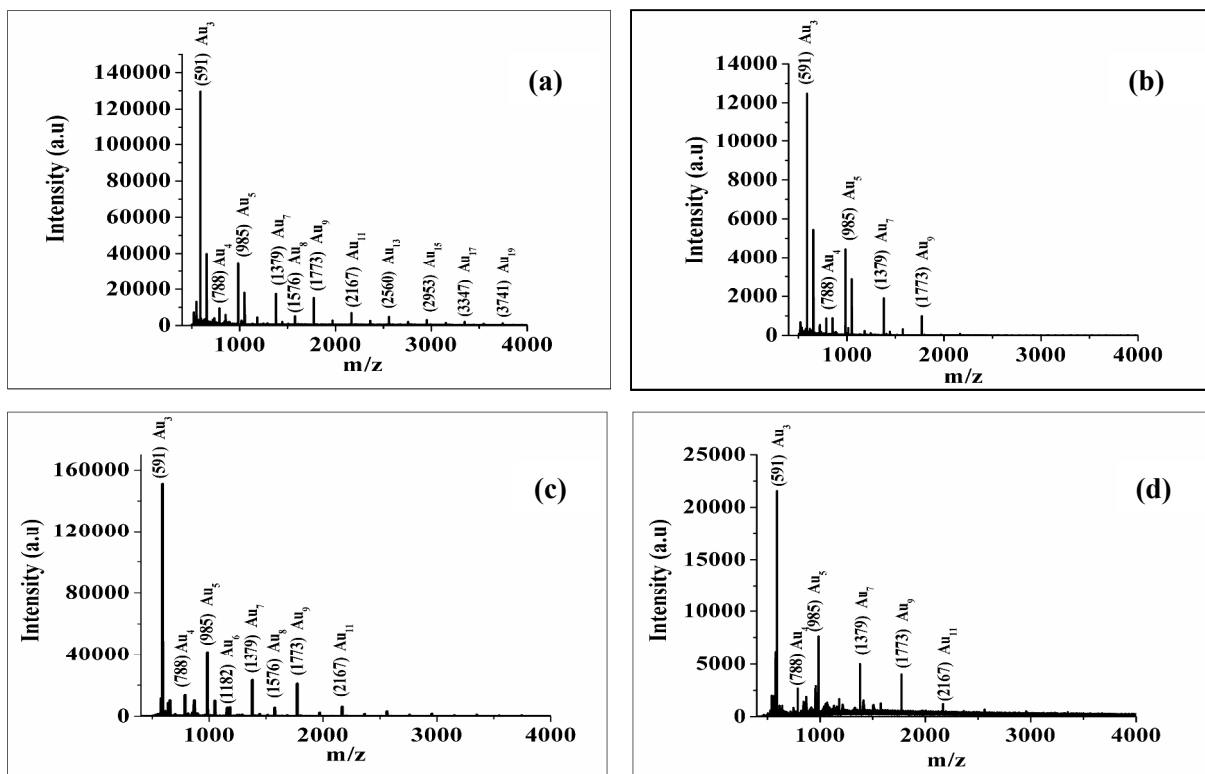
Figure 10. MALDI-TOF Mass Spectra (positive ions) of 5% Au-ZnO prepared at Zn/PEG ratio of (a) 10, (b) 6 (c) 5 and (d)MALDI-TOF Mass Spectra (positive ions) of 1% Au-ZnO prepared at Zn/PEG ratio of 5.

3.5. Surface Plasmon Band reveals metallic gold on Au-ZnO nanocomposites

Figure 11 displays the DRS absorption spectra of pure ZnO and Au-ZnO nanocomposites prepared at Zn/PEG ratio of 30. All the spectra of Au-ZnO shows broad peak in the visible region due to the formation of SP band. Though the conduction band is exhibited as a sharp one

at 396 nm due to ZnO semiconductor, the presence of SP band is the main characteristic property of Au nanoparticles. There is a blue shift as well as an increase in the plasmon intensity on increasing the Au concentration. A weak plasmon band formation is visible for the initial low concentration of Au. A distinctly broad and blue shifted band was observed in 5% Au-ZnO with a shift from 540 nm to 480 nm. The blue shift in the absorption spectra is generally observed on the formation of smaller size of nanoparticles.[40] But in these materials the particle size increases with [Au]. This can be explained due to the transfer of electron from Au to ZnO to form a uniform fermi energy level during the formation of the Au-ZnO junction, as Au has a higher fermi energy level than ZnO, which subsequently increases the energy separation between the valence band and conduction band and hence the blue shift. The broadening of the SP absorption is possibly due to the formation of gold nanoparticles and different clusters from Au_3 to Au_{19} each one having slightly altered wavelength. Figure S5 displays the DRS absorption spectra of 5% Au-ZnO prepared at different fuel ratio. It was observed that the intensity of SP band increases with the increase of fuel and attain maximum at Zn/PEG ratio of 6. Further increase in the fuel concentration does not lead to the increase in the SP band intensity. The SP band was drastically reduced at Zn/PEG ratio of 3. This indicates the saturation point of the fuel concentration. We also observed the presence of SP band using glycine as a fuel, however the intensity was much less compared to the one made from PEG. Thus PEG acts as a better fuel than the glycine in our present studies.

Though we have done all our experiments with calcined samples it is interesting to note that calcination improves the quality and intensity of the conduction band with minimum change in the plasmon band as exemplified by Figure S6 in SI. Probably this may be due to the fact that ZnO crystals after calcination are free from any defects.
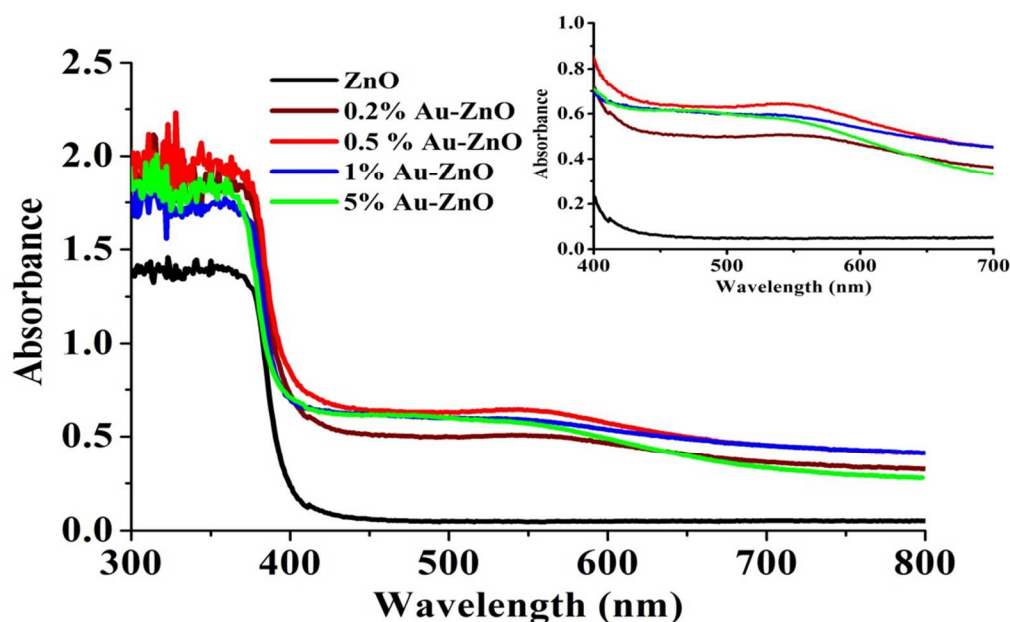
Figure 11. DRS UV-Vis spectra of pure and Au-ZnO nanocomposites at Zn/PEG ratio of 30. The insert showing a compressed spectrum is intended to bring out the clarity of SP band.

3.6. Photoluminescence shows only exciton recombination

The PL spectra of   pure ZnO and Au-ZnO nanocomposites prepared at Zn/PEG ratio of 30 are shown in Figure 12 (a). ZnO generally shows two emission peaks, one in the UV region and another in the visible region[41] the former attributed to exciton recombination and the latter to their defects emission mostly due to Zn interstitials and O vacancies. The main peak was observed at 370 nm. In our present studies, absence of defect emission indicates that ZnO is in pure form without any defect. Absence of defects is also supported by the EPR results. Upon increasing the amount of Au, the intensity of UV emission in both cases of Zn/PEG ratios at 30 (Figure 12 (a) and (b)) was observed to increase up to reaching a maximum at 1% and thereafter with 5% Au it decreases substantially by about 50% and 88% respectively with respect to 1% emission, with the emission continuously getting blue shifted. The blue shift observed here is similar to the same observation in absorption mode.

PL spectra corresponding to Zn/PEG ratio of 5 shown in Figure.12(b) reveal the considerable quenching of PL intensity of ZnO on the addition of 5% Au, even lower than that of pure ZnO. Furthermore, the emission intensity of pure ZnO in the latter experiment i.e. at Zn/PEG=5 is almost 4 times as much as that in the ratio of 30. Wang and coworkers have reported the enhancement in the UV emission of ZnO on the addition of Au.[42] This was explained due to the transfer of electron from Au to ZnO to form a uniform fermi energy level during the formation of the Au-ZnO junction, as Au has a higher fermi energy level than ZnO, which subsequently increases the electron density in the conduction band leading to an increase in the hole-electron recombination rate, thus enhancing the UV emission of ZnO-Au NC. Yet another interpretation comes from the work of Liu *et al.*[43] who reported that the ZnO with a strong band edge emission around 380 nm with no defect emission, and their band edge emission was increased by 12 fold on capping with Pt. The enhancement was explained due to the cross-coupling between spontaneous recombination in ZnO and SP arising from Pt interface. It has been observed in the XRD data that at low Au concentration, both Au and ZnO are present on the surface of Au-ZnO nanocomposites, whereas at high Au concentration, surface was mostly occupied by Au nanoparticles/clusters and a lesser amount of ZnO are visible on the surface of Au-ZnO nanocomposites (See Figure 7 as an example). The transfer of electron between metal and ZnO occurs through the unction on the surface.[44] Therefore, up to the level of 1% Au, the enhancement in PL intensity was observed due to the transfer of electron through SP band coupling between Au and ZnO. However, the PL intensity was quenched in 5% Au which is due to the reduced electron transfer process between Au and ZnO since the presence of ZnO on the surface of the nanocomposite was lower at 5% Au.

This can also be explained according to the Lakowicz model[45] as well as the suggestion by Michael *et al.*[32] According to Lakowicz's radiating plasmon model,[45] the bigger particle size

prefer surface plasmon resonance (SPR) scattering of metal that could lead to PL enhancement, while the smaller particle size prefer SPR absorption which quenches the PL emission. In our case, ZnO surface is covered by NP's and clusters. The first portion of this model is applicable to our case up to 1% since the particle size increases from 8.5 nm to 13.2 nm. However, on increasing the [Au] to 5% there is a considerable quenching to the extent 88% and 50% with the particle size increasing to 15.5 nm at the Zn/PEG ratios of 5 and 30 respectively This can be explained by the model of Michael *et al.*[32] who observed the same kind of blue shift as well as quenching in PL intensity of ZnO on the addition of 5% Ag. They suggested that the silver clusters formed on the surface reduced the intensity of ZnO emission due to scattering of the incoming radiation by the increased amount of silver clusters as well as the unavailability of ZnO surface for effecting the PL emission. This argument is supported from our MALDI data, where formation of Au cluster with a maximum intensity was observed in 5% Au-ZnO prepared at Zn/PEG ratio of 5 and no Au cluster formation in samples prepared at Zn/PEG ratio of 30 with 5% Au. The latter has gold NP's and AuClO as seen from XRD data.
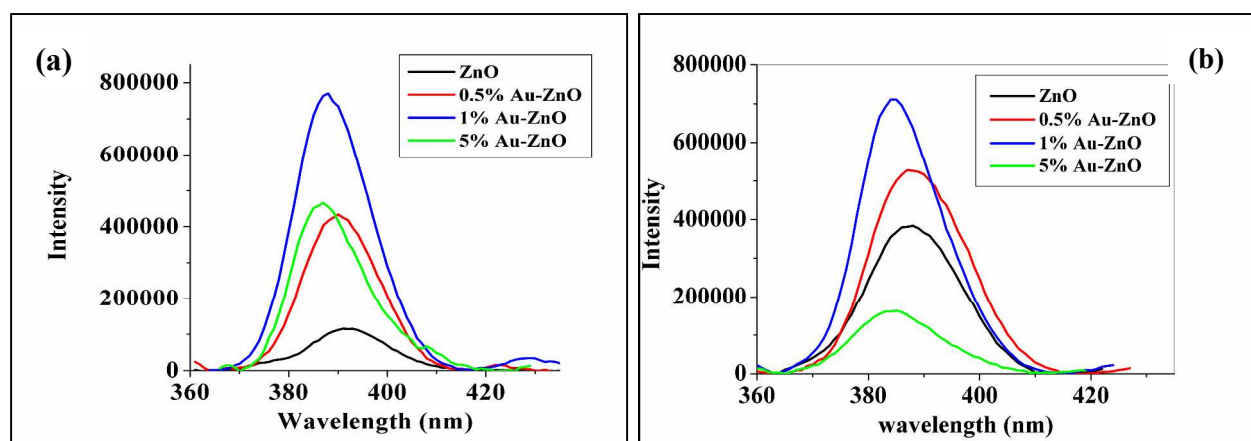

Figure 12. Photoluminescence spectra of pure and Au-ZnO nanocomposites prepared at Zn/PEG ratio of (a) 30 and (b) 5.

3.7. Catalytic Activity of Au-ZnO nanocomposites

To determine the catalytic activity of Au-ZnO, the reduction of nitro compound into amino derivative, i.e., 4-Aminophenol with $NaBH_4$ was studied. Similar studies with Au/Ag clusters have been reported by other earlier workers.[29,46,47] Our experiments were carried out in the absence and presence of ZnO as well as Au-ZnO. It can be seen from Figure 13 that 4-NP shows an absorption peak at 317 nm and on the addition of $NaBH_4$, a red shift from 317 to 400 nm was observed, in a manner similar to earlier reports, revealing the formation of 4- Nitrophenolate ion in the alkaline medium. In the absence of Au-ZnO, there was no change in the spectrum, that is, the addition of pure ZnO did not affect the absorption spectrum, beyond the detection of already formed Nitrophenolate anion which remains unchanged. This suggests that pure ZnO doesn't show any catalytic activity though it possesses free electrons from the conduction band. However, the reduction of 4-NP was clearly observed on the addition of 5% Au-ZnO prepared with Zn/PEG ratio of 5. At 10 min, 4-NP was reduced up to 50% along with the formation of a new peak at 300 nm (low intensity) and emergence of a new large intensity doubly split band at 250-257 nm. A 65% reduction was observed at 20 min and there was no further reduction of 4-NP after 20 min. The characteristic peaks of 4-Aminophenol have been observed at 300 nm (lower intensity) and a larger intensity 230 nm.[48] The prominently split peaks at 250-257 nm in our observation are not part of 4-Aminophenol and hence must be from an intermediate or definitely a product different from 4-Aminophenol. Inset of Figure 13 show the enlarged UV-Visible spectra between 200-300 nm. Furthermore a closer observation of the spectral data of Leelavathi et al.[29] indicates the formation of this peak (~250nm) in very small intensity along with the large intensity 230 and 300 nm peaks characteristic of 4-Aminophenol. Similarly in yet another interesting observation, the same above referred 20 minutes reaction in presence of Au-ZnO with Zn/PEG ratio of 5 there is a small formation of the peak at 230 nm and 300 nm due to
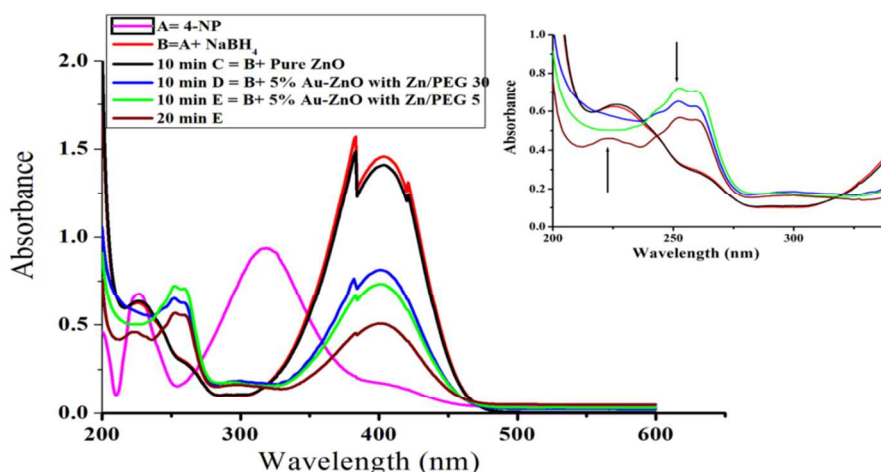
4-Aminophenol. A complete reduction of 4-NP at 18 min with Ag clusters as a catalyst with faster (increased) reduction at higher temperature has been reported by Leelavathi et al.[29] However in our present studies the reduction reaction remains unchanged after 20 min and reaction at higher temperature does not increase the reduction process any further. Another notable observation is that an addition of 5% Au-ZnO prepared with Zn/PEG ratio of 30 also shows reduction of 4-NP up to 49% at 10 min showing only the split peaks at 250-257 nm with no sign of the presence of peaks at 230 nm characteristic of 4-Aminophenol. MALDI results of this Au-5% Au-ZnO prepared with Zn/PEG of 30 reveals the total absence of Au cluster though the presence of Au-particles is displayed by XRD. If reduction of 4-NP depends only on Au cluster, then we should not observe any reduction of 4-NP in the presence of 5% Au-ZnO with Zn/PEG of 30. This suggests that the catalytic activity of Au-ZnO to convert 4-NP into the species having a doubly split peak 250-257 nm is due to the bulk Au nanoparticles deposited on ZnO. It can be seen from TEM image that Au exists in the form of both Au nanoparticles and clusters and the existence of Au in the form of bulk nanoparticles dominant over Au clusters. Furthermore, the observation from our 20 minutes experiment showing the presence of a chunk of the unknown species having the 250-257 nm peaks and at the same time a small formation of 4-Aminophenol reveals clearly that the first reduction process involving the formation of 250-257 nm peaks is catalyzed by the Au-nanoparticles while further reduction to 4-Aminophenol is catalyzed by Au clusters as seen by a comparison of results from 5% Au-ZnO from ZnO/PEG ratios of 30 and 5 respectively. MALDI results come to our support by proving that the former does not have any clusters while the latter has clusters along with Au-nanoparticles. The mechanism of the catalytic reduction to form the first or "intermediate species", represented by 250-257 nm peaks, is from the conversion of 4-Nitrophenolate ion to the "intermediate species" on the surface of Au nanoparticles, which allow the transfer of electron from BH_4^- to

Nitrophenolate ion via Au nanoparticles. The final reduction to 4-Aminophenol is catalyzed by Au cluster which is present as a minor constituent in presence of a larger amount of Au-nanoparticles in our studies. As for the species exhibiting the 250-257 nm peaks we suggest that it should be due to 4-Aminophenolate anion just by comparing the spectral shift of 4-NP to Nitrophenolate anion on the one hand with that of 4-Aminophenol to 4-Amnophenolate anion. We, therefore, propose the following catalytic mechanism (Scheme 1) for the reduction of 4-Nitophenol to 4-Aminophenol.
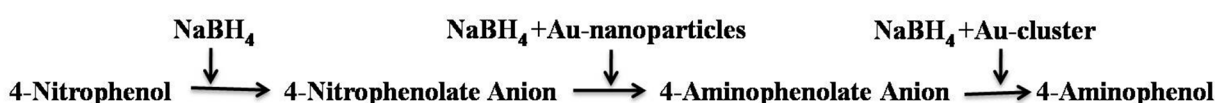
Scheme 1. Mechanism for reduction of 4-NP to 4-Aminophenol using Au/ZnO as catalyst.

It must be said that we could not get a UV-Vis spectrum of 4-Aminophenolate anion in the literature though there is a reference by Ghosh *et al.*[49] to the formation of complexes of Fe(II), Ni(II), Zn(II) and Cu(II) with this 4-Aminophenolate anion.

Figure 13. UV-visible spectra of the reduction of 4-NP with NaBH₄ in the presence of Au-ZnO nanocomposites at different time interval. Inset: Enlarged UV-Visible spectra showing time dependent formation of intermediate (↓) 4-aminophenolate anion 4-Aminophenol (↕).

3.8. *In vitro* cytotoxicity by gold nanoparticles/ clusters reveals cancer cell destruction

One of the most significant observations from the study of gold nanoparticles/clusters with or without attachment to other molecules is its relevance and importance to biology. Two outstanding reviews on the subject of gold nanoparticles in general and in biology come from Sperling and coworkers[50] and Webb and Bardan.[51] While the first one points to their use in labelling, delivering, heating and sensing the latter one pertains to the use of gold NP's as an agent for targeting, imaging, therapy and theranostics (therapy + diagnostics). Because of the nontoxic property of gold particles they have become powerful nanoagents for cancer detection and treatment. In fact our own work relates their possible use for cancer treatment (though it could also be used as tool for diagnostics, currently under investigation). We are here highlighting only their anticancer activity in terms of cell viability towards the MCF-7cell lines being reported as the first part of our larger strategy. First we agree to the fact that cellular impact of nanomaterials *in vitro* may be difficult to implicate them to the real situation of *in vivo* though *in vitro* study is the first step to take them to the real situation. It should be noted that the nanoagents that we use here are also colloidal nature with nano gold particles on the surface of ZnO nanocrystals i.e. in the form of Au/ZnO nanocomposites dispersed in the same medium as for the cell lines. It is important to note that ZnO itself has limited anticancer properties[52-55] and in addition they are nontoxic, in other words they do not affect the normal cells as elegantly pointed out in the work of Akhtar *et al.*[52]

We have already established the nature of the nanoparticles/clusters, i.e. n% Au/ZnO where n varies from 0.0 to 5% of input gold. They have been synthesized by solution combustion methodology using different Zn/PEG ratios as another parameter, wherein PEG was used as fuel. This ratio along with the percentage of gold initially added to ZnO tend to vary the composition of these nanoagents which contain different clusters and nanoparticles. The composition of these

Au/ZnO nanoparticles and Au atomic clusters have been clearly brought out earlier by various characterization methods. Hence the parameters that will play a role in the destruction of cancer cells i.e. cytoxicity are (i) percentage of Au, (ii) ZnO/fuel ratio (iii) the quantity of these anticancer agents and (iv) their particle size; the nanoagents were made and characterized and *in vitro* cytotoxicity studies were done strictly adhering to the procedure mentioned in section 2.3. Table 1 summarizes the current results obtained by the *in vitro* assay for cytotoxic activity (MTT assay). The measurements were duplicated to ensure repeatability. In addition it must be noted that the average particle size measured from XRD are 8.5, 10.0, 12.3, 13.2 and 15.5 nm respectively for ZnO, 0.2% Au/ZnO, 0.5% Au/ZnO 1.0% Au/ZnO and 5% Au/ZnO samples though the actual % Au is less than the input(see section on SEM). A comparison of percentage cell viability, i.e the percentage of live cells on being treated with a certain concentration of these nanoagents shows that 1% Au/ZnO has the best efficiency in destroying 88% of the cancer cells, even with a small amount of 200 μg/ml of nanoagent acting on a colony of 10^5 cells. It is, however, interesting that a substantial increase in gold concentration, by using the same amount of 200 μg/ml of 5% Au/ZnO shows a slightly decreased efficacy (82% cell viability) though it is far better than the same concentration of pure ZnO. This reveals that gold either in the form of clusters or nanoparticles (NP's) must have a critical role in reducing this observed cancer cell viability. With this limited data it is suspected or logically inferred that either an increase in the concentration of 1% Au/ZnO to about 250 μg/ml or increasing the gold percentage to either 1.5 or 2% Au but maintaining the concentration at 200 μg/ml of 1.5-2% Au/ZnO or increasing the incubation time to 72Hrs could have led to complete destruction of cancer cell. Detailed work on this is under process. Figure.S7 (supporting information) represents the data in the form of a histogram for quick comparison. It may be noted that a control experiment was done with 3T3

fibroblast cell lines with a maximum concentration of 250 μg/ml, which is found to be biocompatible.

Yet another difference is in the comparative rate of reduction in cell viability as shown in Figure.14. In smaller amounts until about 12 μg/ml of pure ZnO performs better than the other two concentrations in cell destruction. This may be because of the easier entry of pure ZnO into the cell membranes since its particle size is the least compared to those of 1% and 5%Au on the surface of ZnO. Smaller particles may find it easier to attach themselves to the cell wall membranes to form vesicles which then can be attacked by lysosomes leading finally to necrosis or mitocondrial damage. However, it has been found earlier that interactions between different types of nanoparticles and cells are functions of size, shape and surface chemistry of nanomaterials.[56]   Though it is true that pure ZnO has a size-wise advantage other factors are even more important. Charged nanoparticles displayed higher toxicity compared to neutral particles.[57] Surface charge of gold nanoparticles has been observed to mediate the mechanism of toxicity. Goodman and coworkers[58] have noted that toxicity of gold nanoparticles functionalized with cationic and anionic side chains are superior to that of neutral Au NP's. In addition, it was noted that in certain cases cationic AuNP's display a moderate toxicity while their anionic counterparts has no toxicity. In general all earlier observations[59,60] indicate Au NP toxicity towards cancer cells has the order, positively charged NP's > negatively charged NP's > neutral NP's. In case of such neutral NP's one does it better by adding a capping agent or 'carrier agent'; for example for certain Au NP's, cetyl tetramethylammonium bromide (CTAB) has been used as a capping agent.[61]

In our experiments, gold NP's and clusters in 1%Au/ZnO and 5%Au/ZnO (actual values gold being much less than the introduced amount; see SEM section) present on the surface of ZnO seem to facilitate attachment to membrane walls through gold rather than ZnO. In other

words, the presence of gold in the other two cases speeds up the efficacy of cell destruction. This contention finds support from the fact that pure ZnO seems to saturate at 200 µg/ml (46% cell viability). Hence, the lower cell viability i.e. greater cell destruction by 1% Au/ZnO and 5% Au/ZnO needs an explanation other than just the particle size noting that all three samples were made under the same conditions of ZnO/PEG ratio of 5. Pure $Zn^{\delta+}O^{\delta-}$ is an ionic crystal which is hexagonal in shape. Within the crystal structure Zn is present as a ZnO_4 tetrahedral moiety with more of oxygens on the surface. Strictly speaking the surface of ZnO is negative in character while the depositing gold being a metal sits on the surface of ZnO through the forces of electrostatic interaction creating a charge distribution of the kind $(ZnO)^{\delta-}(Au_n)^{\delta+}$ where n=1 refer to NP's and n= 3, 5, 7, 9, 11 to clusters(*vide supra*). These ionic NP's move towards the cell membrane walls with gold pointing towards the wall for getting off-loaded either as Au losing its ZnO counterpart because of the poor binding energy due to simple and small electrostatic interaction between them. Then, of course, gold NP's and clusters become part of the vesicle which will be attacked by lysosome with subsequent mechanism[62] leading to necrosis or mitochondrial damage *viz.* cell death. OR the entire $(ZnO)^{\delta-}(Au_n)^{\delta+}$ may go inside the cell through the vesicle formation by interacting with lysosomes either separately as ZnO and Au_n or

**Table 1. Results on anticancer activity on Au/ZnO nanoagents on MCF 7 cell lines****

Concentration in µg/ml	% Of Cell Viability		
	(a) Pure ZnO*	(b) 1%Au/ZnO*	(c) 5%Au*
6	84.28 ± 2.77	93.33 ± 4.27	94.08 ±0.45
12	74.92 ± 0.62	78.3 ± 3.3	82 ± 0.57
25	68.56 ± 1.70	47.89 ± 57	59.72 ± 0.62
50	60.76 ± 3.56	41.88 ± 1.08	42.84 ± 1.41
100	51.96 ± 0.17	36.34 ± 1.94	29.92 ± 1.47
200	46.44 ± 1.30	12.29 ± 2.91	18.24 ± 1.92

    * Same Zn/PEG ratio of 5.   ** each well contains 10^5 cells

together as $(ZnO)^{\delta-}(Au_n)^{\delta+}$. Pure ZnO having a negatively charged surface will have a lesser interaction with cells than the ZnO bearing 1% and 5% Au with a positive head. A look at Figure.14 indicates the preference for the entry of $^-(Au_n)^{\delta+}$ into the membrane leaving behind $(ZnO)^{\delta-}$. Now it is clear that between the particle size and charge on the nanoagent the latter plays a significant role. Moreover, if as suggested by us the separation of gold NP's and clusters - $Au_3,$ $Au_5,$ $Au_7,$ Au_9 and Au_{11}- occur inside the cell membrane wall their sizes are considerably smaller than that of pure ZnO nanorods. Since among the clusters, $[Au_3]$ is much higher in number it is suggested that both the NP's and Au_3 and possibly Au_5 may have played a larger role in *in vitro* cell toxicity.
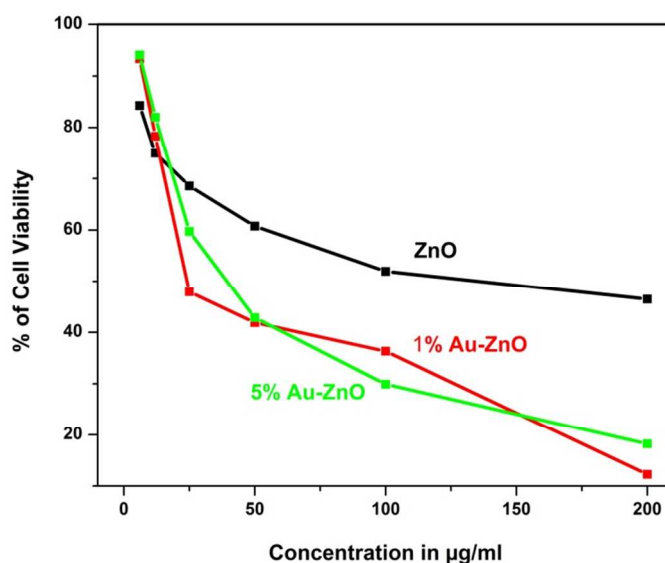
Figure 14. A graphical representation of %cell viability for three samples prepared under the same Zn/PEG ratio of 5.

In order to identify the contributing factor for cell destruction, i.e. ZnO or Au NP's or Au clusters a cell viability was again tested with 5% Au/ZnO prepared with differing ZnO/fuel ratios 30 and 5 and compared with pure ZnO and 1% Au/ZnO prepared with ZnO/Fuel ratio of 5, restricted to the use of up to 100 μg/ml concentration as shown in Table 2. 5% Au/ZnO prepared with the highest ZnO/PEG ratio of 30 have no gold clusters at all, but has $(AuClO)_2$ type of

clusters (see Figure. 9 (b)) along with definite presence of Au NP's as proved by XRD data. So the destruction of cells must have been caused by either ZnO or by a combination of ZnO and $(AuClO)_2$ or by the gold NP's. However, the cell viability value for the concentration of 100 µg/ml decreases in the order pure ZnO > 5% (30) > 5% (5). This means that higher contribution to cell destruction comes from gold, in the form of either clusters or particles. A comparison between the latter two i.e., 5% (30) > 5% (5) reveals that the former has no clusters at all but only NP's and the latter has clusters in addition to NP's having greater cell destroying capability. However, very small difference in the cell viability data between them leads us to suggest that both NP's and Au clusters, particularly smaller clusters like Au_3 and Au_5, play dominant roles. A comparison of 5% (5) and 1% (5) in Table 2 substantiates our conclusion that nanoparticles and clusters play the common role in the destruction of cancer cells. This is based on the fact that Au_3 clusters are found as 6 times as much in 5% (5) as in 1% (5) based on MALDI data though the induction of gold is 5 times as much in the latter. However, more work with additional closer parameters is needed to provide a clear mechanism vis-à-vis the differential contributions from ZnO, and gold clusters and NP's. But the most important conclusion that Au/ZnO nanoagents have definite anticancer activity at its very low concentration cannot be denied. In addition this is the first report of its kind where a carrier or a coupling system for the Au nanoparticle is a simple molecule like ZnO which itself is toxic to cancer cell though to a much lesser extent and is simultaneously nontoxic to normal cells.

A comment on the anticancer property of pure ZnO is in order. Though the cell viability is around 40% with saturation at this point in our work the same seems to be so in earlier studies[55-58] as can be seen from (supporting info T3) though the cells tested are different.

Table 2. Results on anticancer activity on 5%Au/ZnO nanoagents prepared under different ZnO/PEG ratios.

Concentration in µg/ml	% Of Cell Viability			
	Pure ZnO(5)[*$]	5% (30)*	5% (5)*	1% (5)*
6	84.28 ± 2.77	96.88 ± 3.54	95.31 ± 3.09	92.19 ± 2.21
12	74.92 ± 0.62	92.50 ± 3.54	87.81 ± 1.33	80.00 ± 2.65
25	68.56 ± 1.70	67.50 ± 2.65	62.19 ± 3.09	46.25 ± 1.77
50	60.76 ± 3.56	45.31 ± 3.09	48.75 ± 2.65	38.13 ± 1.77
100	51.96 ± 0.17	39.06 ± 4.86	36.56 ± 3.98	30.94 ± 1.33
200	46.44 ± 1.3	---	18.24 ± 1.92	12.29 ± 2.91

$ as in Table 1; * Numbers in parenthesis corresponds to Zn/PEG ratio with % indicating Au content.

3.9. Mechanism for the formation of Au clusters

The formation of Au cluster entirely depends on the amount of PEG as well as $HAuCl_4^-$ used during preparation. At low PEG, upto 1% Au, bulk Au nanoparticles as well as small amount of Au clusters were being formed on the surface of ZnO. At 5% Au, in addition to bulk Au nanoparticles, AuClO clusters were also formed and no formation of Au clusters. As soon as the PEG concentration was increased, Au cluster in addition to the bulk Au nanoparticles were formed on the surface of ZnO. Odd number Au clusters are dominant with the presence of lesser quantities of even numbered ones. We can infer from this observation that initially AuClO was formed at low supply of energy. At the expense of high energy during combustion process, most of the Cl was removed from AuClO to form Au clusters. Schematic representation of the formation of Au cluster is shown in scheme 2.
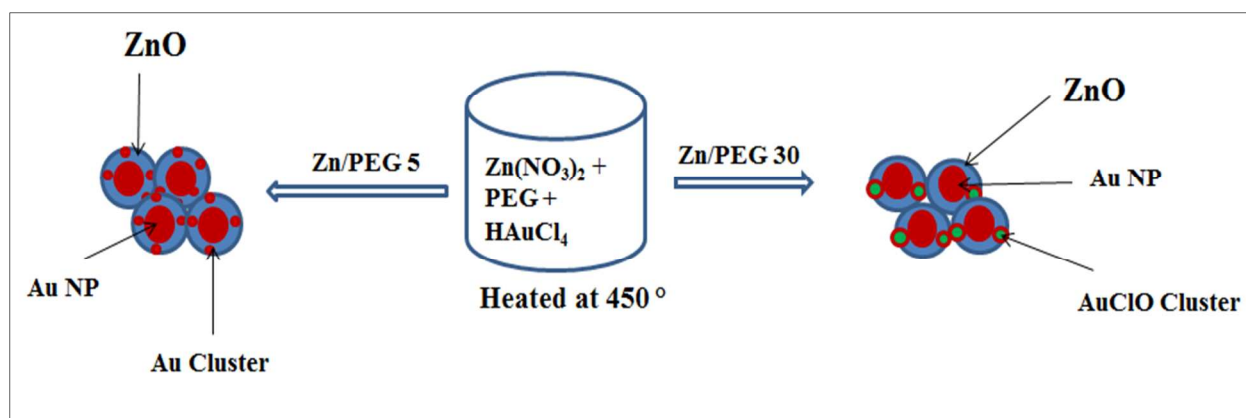
Scheme 2 Schematic representation of the formation of Au clusters.

4. Conclusion

In conclusion, fuel dependent Au clusters were prepared by tailoring the Zn/PEG ratio using a solution combustion synthesis. Only at high PEG, Au clusters was formed with the major peak at Au_3 clusters. Low supply of energy causes the formation of $(AuClO)_2$ clusters instead of Au_n clusters with n being even and odd with the dominant presence of odd numbered ones. There is a simultaneous existence of nanoparticles and clusters. The PL mechanism of Au-ZnO depends on the surface and size of the particles. The electron transfer from Au to ZnO occurring at the surface enhances the PL of ZnO and the presence of Au clusters seems to quench the ZnO emission. The catalytic effect on reduction of 4-NP with an intermediate as 4-Aminophenolate anion was promoted by bulk Au nanoparticles and conversion into 4-Aminophenol by Au clusters. This study demonstrates the simple synthetic method to produce desired Au clusters just by tailoring fuel ratio and percentage of doping. The most important contribution of this work is that Au/ZnO nanoparticles and clusters act as anticancer agents. In addition this is probably the first report of its kind where a carrier or a coupling system for the Au nanoparticle is simple molecule like ZnO.

References

1. M. J. R. Vazquez, M. C. Blanco, R. Lourido, C. V. Va´zquez, E. Pastor, G. A. Planes, J. Rivas and M. A. L. Quintela, *Langmuir*, 2008, **24,** 12690-12694.

2. M. Ganguly, A. Pal, Y. Negishi and T. Pal, *Langmuir*, 2013, **29,** 2033-2043.

3. T. M. Wallis, N. Nilius and W. Ho, *Phys. Rev. Lett.*, 2002, **89,** 236802-4.

4. J. P. Wilcoxon and B. L. Abrams, *Chem. Soc. Rev.,* 2006, **35,** 1162-1194.

5. P. Schwerdtfeger, *Angew. Chem. Int. Ed.,* 2003, **42,** 1892-1895.

6. M. Li, D. P. Yang, X. Wang, J. Lu and D. Cui, *Nanoscale. Res. Lett.*, 2013, **8,** 182-186.

7. C. A. J. Lin, T. Y. Yang, C. H. Lee, S. H. Huang, R. A. Sperling, M. Zanella, J. K. Li, J. L. Shen, H. H. Wang, H. I. Yeh, W. J. Parak and W. H. Chang, *ACS Nano,* 2009, **3,** 395-401.

Physical Chemistry Chemical Physics Accepted Manuscript

8. J. Zheng, J. T. Petty and R. M. Dickson, *J. Am. Chem. Soc.,* 2003, **125,** 7780-7781.

9. S. Link, A. Beeby, S. F. Gerald, M. A. E. Sayed, T. G. Schaaff and R. L.Whetten, *J. Phys. Chem. B.,* 2002, **106,** 3410-3415.

10. R. M. Olson, S. Varganov, M. S. Gordon, H. Metiu, S. Chretien, P. Piecuch, K. Kowalski, S. A. Kucharski and M. Musial, *J. Am. Chem. Soc.,* 2005, **127,** 1049-1052.

11. X. Huang, I. H. E. Sayed, W. Qian and M. A. E. Sayed, *J. Am. Chem. Soc*., 2006, **128,** 2115-2120.

12. M. Brust, M. Walker, D. Bethell, D. J. Schiffrin and R.Whyman, *J. Chem. Soc. Chem. Commun.,* 1994, 801-802.

13. S. Rath, S. Nozaki, D. Palagin, V. Matulis, O. Ivashkevich and S. Maki, *Appl. Phys. Lett.,* 2010, **97,** 053103-3.

14. E. S. Shibu, B. Radha, P. K. Verma, P. Bhyrappa, G. U. Kulkarni, S. K. Pal and T. Pradeep, *ACS Appl. Mater. Interfaces,* 2009, **10,** 2199 -2210.

15. Y. Negishi, K. Nobusada and T. Tsukuda, *J. Am. Chem. Soc.,* 2005, **127,** 5261-5270.

16. W. Kurashige, S. Yamazoe, K. Kanehira, T. Tsukuda and Y. Negishi, *J. Phys. Chem. Lett.,* 2013, **4,** 3181-3185.

17. H. Wei, Z. Wang, L. Yang, S. Tian, C. Hou and Y. Lu, *Analyst.*, 2010, **135,** 1406-1410.

18. K. Rajeshwar and N. R. D. Tacconi, *Chem. Soc. Rev.,* 2009, **38,** 1984-1998.

19. K. Nagaveni, M. S. Hegde, N. Ravishankar, G. N. Subbanna and G. Madras, Langmuir, 2004, **20,** 2900-2907.

20. J. Z. Marinho, F. C. Romeiro, S. C. S. Lemos, F. V. Motta, C. S. Riccardi, M. S. Li, E. Longo and R. C. Lima, *J. Nano Mat.,* 2012, 427172-8.

21. C. C. Hwang, T. Y. Wu, J. Wan and J. S. Tsai, *Mater. Sci. Eng. B.,* 2004, **111,** 49-56.

22. F. Deganello, L. F. Liotta, G. Marcı, E. Fabbri and E. Traversa, *Mater. Renew. Sustain. Energy,* 2013, **2,** 8-22.

23. K. Okamoto, I. Niki, A. Shvartser, Y. Narukawa, T. Mukai and A. Scherer, *Nature Mater.,* 2004, **3,** 601-605.

24. X. D. Zhou, X. H. Xiao, J. X. Xu, G. X. Cai, F. Ren and C. Z. Jiang, *EPL*, 2011, **93,** 57009-57014.

25. M. K. Lee, T. G. Kim, W. Kim and Y. M. Sung, *J. Phys. Chem. C.,* 2008, **112,** 10079-10082.

26. S. Yun, J. Lee, J. Yang and S. Lim, *Physica. B.,* 2010, **405,** 413-419.

27. C.T. Ko, Y. Y. Han, C. H. Chen, J. Shieh and M. J. Chen, *J. Phys. Chem. C.,* 2013, **117,** 26204-26212.

28. K. Layek, M. L. Kantam, M. Shirai, D. N. Hamane, T. Sasaki and H. Maheswaran, *Green Chem.,* 2012, **14,** 3164-3174.

29. A. Leelavathi, T. U. B. Rao and T. Pradeep, *Nanoscale Res. Lett.,* 2011, **6,** 123-131.

30. S. Praharaj, S. Nath, S. K. Ghosh, S. Kundu and T. Pal, *Langmuir,* 2004**, 20,** 9889-9892.

31. N. Pradhan, A. Pal and T. Pal, *Langmuir,* 2001, **17,** 1800-1802.

32. R. J. V. Michael, S. Balaji, T. Muthukumar, M. J. Umapathy and P. T. Manoharan, *Phys. Chem. Chem. Phys.,* 2014, **16,** 8541.

33. T. Mosmann *J. Immunol. Methods,* 1983, **65(1–2),** 55–63.

34. Z. Wu, J. Chen and R. Jin, *Adv. Funct. Mater.,* 2011, **21,** 177-183.

35. F. J. Sheini, R. Yousefi and K. R. Patil, *Ceram. Int.,* 2012, **38,** 6665-6670.

36. L. K. Ono and B. R. Cuenya, *J. Phys. Chem. C*., 2008, **112,** 4676-4686.

37. M. Hohne, *Phys. Stat. Sol.(b).,* 1982, **109,** 525-534.

38. B. Guan, W. Lu, J. Fang and R. B. Cole, *J. Am. Soc. Mass Spectrom,* 2007, **18,** 517-524.

39. H. M. Lee, M. Ge, B. R. Sahu, P. Tarakeshwar and K. S. Kim, *J. Phys. Chem. B.,* 2003, **107,** 9994-10005.

40. J. P. Wilcoxon and P. Provencio, *J. Phys. Chem. B.,* 2003, **107,** 12949-12957.

41. L. Irimpan, V. P. N. Nampoori, P. Radhakrishnan, A. Deepthy and B. Krishnan, *J. Appl.Phys.,* 2007, **102,** 063524-9.

42. X. Wang, X. Kong, Y. Yu and H.Zhang, *J. Phys. Chem. C.,* 2007, **111,** 3836-3841.

43. K. W. Liu, Y. D. Tang, C. X. Cong, T. C. Sum, A. C. H. Huan, Z. X. Shen, L. Wang, F. Y. Jiang, X. W. Sun and H. D. Sun, *Appl. Phys. Lett.,* 2009, **94,** 151102-151102-3.

44. T. H. Lin, T. T. Chen, Ch. L. Cheng, H. Y. Lin and Y. F. Chen, *Opt. Express,* 2009, **17,** 4342-4347.

45. J. R. Lakowicz, *Anal. Biochem*., 2005, **337,** 171-194.

46. A. Shivhare. D. M. Chevrier. R. W. Purves and R. W. J. Scot, *J. Phys. Chem. C.,* 2013, **117,** 20007-20016.

47. A. Shivhare, S. J. Ambrose, H. Zhang, R. W. Purves and R. W. Scott, J. *Chem. Commun*., 2013, **49,** 276-278.

48. T. Premkumar, K. Lee and K. E. Geckeler, *Nanoscale Res. Lett.,* 2011, **6,** 547-559.

49. P. Ghosh, A. Begum, E. Bill, T. Weyhermuller and K.Wieghardt, *Inorg. Chem.,* 2003, **42,** 3208-3215.

50. J. A. Webb and R. Bardhan, *Nanoscale*, 2014, **6,** 2502-2530.

51. R. A. Sperling, P. R. Gil, F. Zhang, M. Zanella and W. J. Parak, *Chem. Soc. Rev.*, 2008, **37,** 1896–1908.

52. M. J. Akhtar, M. Ahamed, S. Kumar, M. M. Khan, J. Ahmad and S. A. Alrokayan, *Int. J. Nanomedicine,* 2012, **7,** 844-855.

53. S. Hackenberg, A. Scherzed, M. Kessler, K. Froelich, C. Ginzkey, C. Koehler, M. Burghartz, R. Hagen and N. Kleinsasser, *Int J Oncol.,* 2010, **37,** 1583-1590.

54. T. Chen, T. Zhao, D. Wei, Y.Wei, Y. Li and H. Zhang, *Carbohydr. Polym.,* 2013, **92(2),** 1124-1132.

55. R. Wahab, N. K. Kaushik, A. K. Verma, A. Mishra, I. H. Hwang, Y. B. Yang, H.S. Shin and Y. S. Kim, *J. Biol. Inorg. Chem.,* 2011, **16(3),** 431-442.

56. A. M. Alkilani and C. J. Murphy, *J. Nanopart. Res.,* 2010, **12,** 2313-2333.

57. N. M. Schaeublin, L. K. Braydich-Stolle, A. M. Schrand, J. M. Miller, J. Hutchison, J. J. Schlagera and S. M. Hussain, *Nanoscale*, 2011, **3,** 410.

58. C. M. Goodman, C. D. McCusker, T. Yilmaz and V. M. Rotello, *Bioconjugate Chem*., 2004, **15(4),** 897–900.

59. S. E. A. Gratton, P. A. Ropp, P. D. Pohlhaus, J. C. Luft, V. J. Madden, , M. E. Napier and J. M. DeSimone, *PNAS,* 2008, **105(33),** 11613–11618.

60. G. Orr, D. J. Panther, J. L. Phillips, B. J. Tarasevich, A. Dohnalkova, D. Hu, J. G. Teeguarden and J. G. Pounds, *ACS Nano* 2007, **1(5),** 463–475.

61. B. Nikoobakht and M. A. El-Sayed, *Langmuir,* 2001, **17(20),** 6368–6374.

62. L. Wang, Y. Liu, W. Li, X. Jiang, Y. Ji, X. Wu, L. Xu, Y. Qiu, K. Zhao, T. Wei, Y. Li, Y. Zhao and C. Chen, *Nano Lett*, 2011, **11,** 772–780.